

Glacial Vermicular Ridge Features on Axel Heiberg Island, Nunavut, Canada

Shannon M. Hibbard^{1,2}, Gordon R. Osinski³, Etienne Godin⁴, Antero Kukko^{5,6}, Chimira Andres⁷, Shawn Chartrand⁸, Anna Grau Galofre⁹, A. Mark Jellinek¹⁰, Wendy Boucher¹¹

¹Division of Earth and Ecosystem Sciences, Desert Research Institute, Reno, Nevada, 89512, USA

²Jet Propulsion Laboratory, California Institute of Technology, Pasadena, California, 91101, USA

³Department of Earth Sciences, University of Western Ontario, London, Ontario, N6A 5B7, Canada

⁴Centre d'Études Nordiques, Université Laval, Québec, Québec, Canada, G1V 0A6

10 ⁵UNITE Flagship, Department of Remote Sensing and Photogrammetry, Finnish Geospatial Research Institute, Espoo, Finland

⁶Department of Built environment, Aalto University, Espoo, Finland

⁷Lassonde School of Engineering, York University, Toronto, Ontario, M3J 1P3, Canada

⁸School of Environmental Science, Simon Fraser University, Burnaby, British Columbia, V5A 1S6, Canada

⁹Laboratoire de Planétologie et Géosciences, CNRS UMR 6112, Nantes, France

15 ¹⁰Department of Earth, Ocean and Atmospheric Sciences, University of British Columbia, V6T 1Z4, Canada

¹¹Department School of Graduate Studies, Trent University, Peterborough, Ontario, K9L 0G2, Canada

Correspondence to: Shannon M. Hibbard (shannon.hibbard@dri.edu)

Abstract. Vermicular Ridge Features (VRFs) comprise a series of ridges and troughs with a circular, sinuous, and anastomosing morphology composed of clast-rich sandy diamict. VRFs were first reported on the south coast of Devon Island, Nunavut, Canada, in the Dundas Harbour region. Here, we document the presence of VRFs near Mokka Fjord on Axel Heiberg Island, Nunavut, Canada. We utilize field observations, ultra high resolution LiDAR, and ground penetrating radar to characterize and compare the morphometry and sedimentology of VRFs near Mokka Fjord to other periglacial, paraglacial, and glacial landforms. VRFs near Mokka Fjord have a diameter ranging from 6 to 37 m and reach up to 1.5 m in height. They comprise clast-rich glaciofluvial sediment and till. A leading periglacial (i.e., segregation ice features/lithalsas) and glacial (i.e., ring-ridge moraines and kame/kettled terraces) origin are presented. We interpret Mokka Fjord VRFs to be an ice-marginal feature resulting from paraglacial ablation of buried glacial ice producing a hummocky ring-ridge moraine comprised of ice marginal and supra- and englacial debris. This formation mechanism would infer a largely polythermal glacial environment with limited water supply. Likely from occasional warm-based periods at the ice margins which may allow sediment output and ice burial from basal ice debris redistribution or the thinning and subsequent burial of snout ice from glaciofluvial outwash.



1 Introduction

The Canadian high arctic and has been subject to glacial and periglacial processes throughout the Quaternary Period. These processes can produce a wide variety of landforms, many of which are/were associated with massive ice. These landforms can often appear morphologically very similar and, thus, be difficult to differentiate. This has led to ongoing debate within the fields of periglacial and glacial geomorphology and is especially difficult considering the Canadian high arctic has only recently undergone deglaciation, making it paraglacial in nature experiencing the effects of both recent glaciation and periglacial modification.

Much of the Canadian high arctic lies in an environment favorable to polythermal and cold-based glaciers, which limits the glacial imprint on a landscape. Therefore, evidence of glaciation might be expected in the form of buried snout/ice-marginal glacial ice susceptible to glacial karst development, hummocky till veneers, glaciofluvial outwash, and kames (O' Cofaigh et al., 2005). However, periglacial processes can lead to hummocky terrain in till and glaciofluvial outwash sediments and produce buried massive ice through ice segregation and injection (French and Harry, 1990), which can become susceptible to thermokarst degradation. For example, the topographic inversion of glacial sediments (Fairbridge, 1968) due to the ablation of underlying glacial ice is a common mechanism for the production of hummocky surfaces in deglaciated landscapes (e.g., Clayton, 1964; McKenzie, 1969; Embleton and King, 1975). This process usually forms a series of landforms characterized by mounds and depressions following the retreat of a glacier and has been observed to create conspicuous circular (e.g., Gravenor and Kupsch, 1959) to sinuous and anastomosing (e.g., Knudsen et al., 2006; Hibbard et al., 2021) morainic ridges. Yet, the ablation of buried non-glacial ice can produce morphologically similar features (e.g., Mackay, 1974; Rampton, 1988; Mollard, 2000), the origin of which can still be a topic of debate (e.g., Watson and Watson, 1974; Ross et al., 2019).

While these features may appear similar in the field, the processes by which these features formed are very different. Both massive buried glacial ice and segregation ice are common across the Canadian high arctic (O'Neill et al., 2019) despite being situated in the continuous permafrost zone. Differentiating between massive ice origins and the associated landform origins are key to understanding the evolution of high arctic landscapes and reconstructing Quaternary environmental conditions. This is especially true in continuous permafrost zones, where the presence of massive segregation ice and periglacial landforms can inform us about climate during deglaciation and affects climate change has in high arctic environments.

We report here on a previously undocumented landform on the east coast of Axel Heiberg Island near Mokka Fjord in Nunavut, Canada, that appears remarkably similar to Vermicular Ridge Features (VRFs) recently identified at Dundas Harbour on Tallurutit (Devon Island) (Hibbard et al., 2021). VRFs comprise a series of ridges and troughs with a circular, sinuous, to anastomosing, and therefore “worm-like,” morphology. We refer to these features as Vermicular Ridge Features (VRFs) as a descriptive term without any genetic interpretation. We provide a comparison of Mokka Fjord VRF morphometrics, substrate



65 characteristics, and associated landforms and processes, to other morphologically similar glacial and periglacial landforms and
present a working hypothesis for the formation of this landform and the implications it has on past climate conditions during
the Holocene.

2 Geologic and Geomorphic Setting

Axel Heiberg Island (Umingmat Nunaat) is located in the Qikiqtani region of Nunavut of Inuit Nunangat in Canada (Fig. 1).
70 It is also part of the Sverdrup Islands in the Queen Elizabeth Islands of the Canadian Arctic Archipelago.
Axel Heiberg Island lies within the thickest section (up to 13 km) of the Sverdrup Basin, which is predominantly composed of
Carboniferous to Paleogene siliciclastics, evaporites, and carbonates (Balkwill, 1978; Russell et al., 2006; Embry and
Beauchamp, 2008; Harrison and Jackson, 2014). Following the Pleistocene glaciations, Quaternary deposits (including stream,
deltaic, glacial, and marine beach sediments) were deposited over bedrock geology, and occupy valley floors and raised beach
75 sediments along the coasts (Thorsteinsson, 1971a, 1971b).

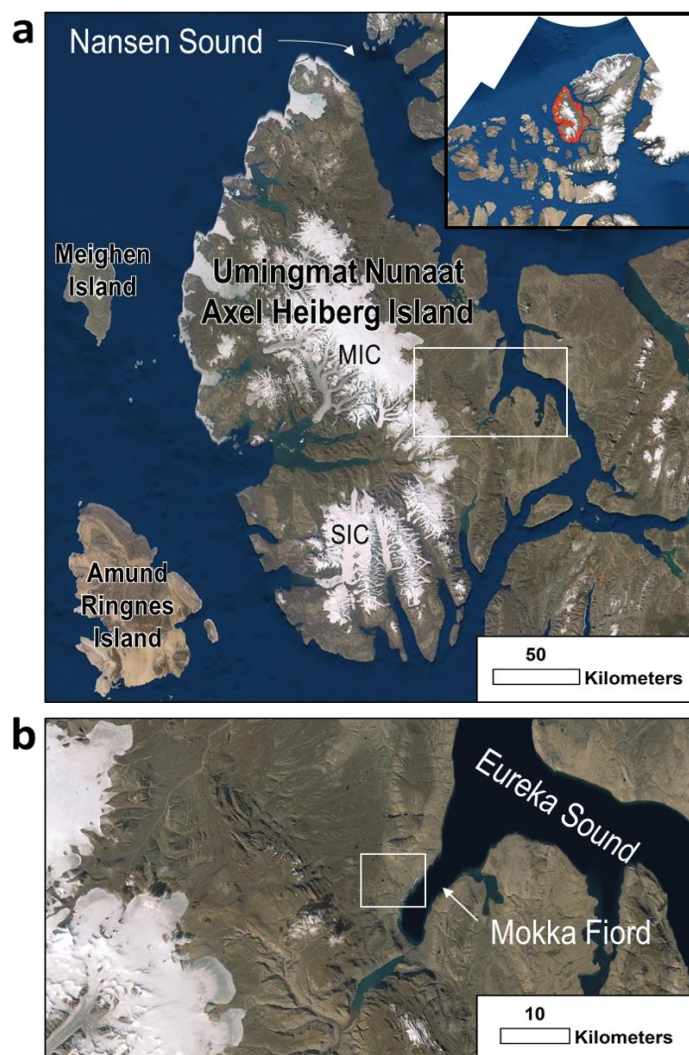
The island hosts two major ice caps, the Müller Ice Cap and Steacie Ice Cap (Fig. 1a), and a wide range of glacier types such
as cirque, outlet, piedmont, and valley glaciers (Ommanney, 1969; Thomson et al., 2011). The thermal regime of glaciers
presently on Axel Heiberg Island are cold and polythermal (Blatter, 1987; Ó Cofaigh et al., 1999) which is thought to have
80 extended into the last glacial maximum with the exception of fjord glaciers interpreted to be warm-based glaciers and ice
streams (Ó Cofaigh et al., 1999; England et al., 2006). Axel Heiberg Island was covered by the Innuitian Ice Sheet, which
reached its last glacial maximum around 29 ka BP (Bednarski, 1998). Extensive deglaciation of the Innuitian Ice Sheet occurred
predominantly from west to east between 16.5 and 11 ka BP and marine-based ice largely disappeared by 9 ka BP leaving
mostly land-based ice on Axel Heiberg and other islands (England et al., 2006). Deglaciation of the island proceeded and freed
85 most of its fjords of ice by 8 ka BP (England et al., 2006) until reaching contemporary conditions around 7.5 ka BP. The marine
limit varies across the Axel Heiberg Island, but has been reported to range between 78 and 158 m asl (e.g., Bednarski, 1998;
Pollard and Bell, 1998; Dyke et al., 2005).

The area of field study (Fig. 1b) lies within the Granite dispersal train (Ó Cofaigh et al., 2000; England et al., 2006) and is
90 composed of Quaternary deposits (Thorsteinsson, 1971a, 1971b). Detailed surveying of VRFs was conducted at one main field
site located on a terrace along a channel trending northwest-southeast feeding into Mokka Fiord. To our knowledge, this field
site has not directly been analyzed for surficial geology and geomorphology in previous studies, but the coast of Nansen Sound
and Flat Sound ~300 km to the northwest was surveyed by Bednarski (1998) who determined the area to be dominated by
meltwater channels sourced from the western highlands, moraines and kame terraces, and marine sediments.

95



Present-day conditions represent a polar desert environment (Andersen et al., 2002). The nearest long-term climate station is Eureka A station located on the coast of Fosheim Peninsula on Mirnguiqirvik (Ellesmere Island) ~ 300 km northeast of the field site. The Eureka A station reports a mean annual air temperature of -18.8°C and a mean annual precipitation of 79.1 mm (mostly in the form of snow—60.3 mm) between 1981 and 2010 (Environment Canada, 2021). Permafrost thickness has been measured to be 400 to 600 m at Mokka Fiord (Taylor and Judge, 1976; Pollard et al., 1999). Although the average climate equates to a polar desert, the Arctic is characterized by some of the most intense summertime climate variability resulting in wet precipitation and glacial/snow melting events (Constable et al., 2022) unlike a polar desert environment.



105 **Figure 1: Axel Heiberg Island observed using World Imagery (Esri, 2018). (a) Axel Heiberg Island is located in Nunavut, Canada (outlined in red on top right). Nansen Sound runs along the east coast of much of Axel Heiberg Island. White box locates panel b. MIC and SIC represent Müller Ice Cap and Steacie Ice Cap, respectively. (b) Location of the field region (located within white box centered at $79.61589, -87.5556$) is northeast of Mokka Fiord, which feeds into Eureka Sound. World Imagery Source: Esri, Maxar, GeoEye, Earthstar Geographics, CNES/Airbus DS, USDA, USGS, AeroGRID, IGN, and the GIS User Community.**



3. Methodology

110 Fieldwork was carried out ~4 km northwest of Mokka Fiord on Axel Heiberg Island in July 2019 (Fig. 1). Field reconnaissance was done on foot and by helicopter which led to the identification of VRFs across multiple terraces along one river channel that feeds Mokka Fiord. A terrace along the channel was selected for in-depth field analysis, including trenching, Light Detection and Ranging (LiDAR), and Ground Penetrating Radar (GPR) data collection to characterize the landforms.

AkhkaR4DW, a backpack mobile laser scanning system was used to kinematically collect high-precision 3D topographic data
115 (Kukko et al., 2012; Liang et al., 2015; Kukko et al., 2017, 2020; Hyyppä et al., 2020). This system was developed by the Finnish Geospatial Research Institute to produce ultra-high resolution (1–5 cm-scale) digital elevation models (DEMs). The positioning of the system relies on post-processed tightly coupled differential processing of data from a GNSS receiver (NovAtel Pwrpak7) observing GPS and GLONASS satellite constellations and an inertial measurement unit (GNSS-IMU, NovAtel ISA-100C). For more details, see Kukko et al., (2020).

120

The lidar point cloud LAS file was produced using RiProcess and TerraScan software to filter and reduce the raw point cloud data which had a total of 46,163,219 points covering an area of ~6.42 ha with an average density of 164.2 points/m². WhiteBox Geospatial Analysis ToolBox (GAT), an open-source geospatial data analysis software developed by Professor John Lindsay at the University of Guelph (Lindsay, 2014, 2016), was used to create a Bare Earth DEM and Hillshade. The Bare Earth DEM
125 was created using an inverse-distance weighting (IDW) scheme. A search distance of 10 cm was used to interpolate the point cloud. The Power (p) exponent was set to the default value of 2. Points that exceeded a slope of 30° from the unmeasured point being calculated were considered an outlier/non-ground point and were not used in the output point-cloud. A grid resolution of 5 cm/pixel was used to provide a high-resolution DEM with reasonably short processing time. The Hillshade azimuth (direction of the sun), measured clockwise from North, was set to 315° (northwest). The altitude (angle of illumination),
130 measured from the horizon to normal, was set to 30°. The Bare Earth DEM and Hillshade files were loaded into ArcGIS Desktop 10.8.1 using a WGS 1984 UTM 16N projection.

A Sensors and Software 250 NOGGIN SmartTow GPR system was used to investigate massive ice and deposit thickness; the instrument was equipped with a 250 MHz antenna. Three GPR lines were collected, three of which lie within the LiDAR data,
135 ranging from 20 to 30 meters in length. Signal velocity was determined based on sedimentology, diffraction hyperbola fitting, and context from trenching in the field, which was determined to be 0.125 m/ns (frozen and unfrozen sand and gravel). Based on this signal velocity, GPR signals penetrated down to roughly 4 m before heavily attenuating. GPR data was collected on July 8, 2019, therefore, the thaw depth is representative of that day of the year, which was measured/estimated at 1–1.5 m.

140 GPR data was analyzed using Sensors and Software's Ekko_Project_5 software. GPR data was dewowed and was amplified with a Spherical Exponential Calibrated Compensation (SEC2) gain and an Attenuation value of 8. Elevation data along each



GPR line was extracted from the LiDAR dataset and added to the GPR data file. This corrects for unreliable depths of key subsurface features, but slightly stretches the upper part of the cross-section image.

4 Observations and Results

145 4.1 Context and Setting of Mokka Fjord VRFs

We identified VRFs on seven terraces along a northwest-southeast trending meltwater channel flowing into Mokka Fjord (Figs. 2–4, and S1, Supp. files), five of which reside on the western side of the channel and two reside on the eastern side. The terraces occur at different elevations, with the uppermost terrace occurring at an average elevation of 166 m on the west side, and the lowermost terrace occurring at 114 m on the east side. An additional 5 VRF sites were identified up and down valley
150 from the investigated terraces by helicopter (Figs. 2 and 3), one of which was located in the floodplain of the stream system (Fig. 3e). VRFs were also observed near Strand Fjord when returning from another field site (Fig. 3g).

The VRFs at Mokka Fjord occur in three surficial geologic units mapped by the Geological Survey of Canada (2022), including (1) terraced sediments (At), comprised of coarse surface sediments and patterned ground, (2) till, morainal sediments,
155 undifferentiated (T.W) comprised of marine reworked glacial diamicton, and (3) colluvial deposits, undifferentiated (C.W) comprised of a heterogeneous mixture of source rocks and grain sizes that are products of mass waste and have patterned ground. Our field observations support these regional interpretations and indicate that all VRFs occur in coarse-grained diamicton that is glacially or glaciofluvially sourced.

160 Polygonally patterned ground and solifluction were observed across the field sites. Ponds of water (Fig. 3e), wet soil (Figs. 3c, d), and thaw slumps (not seen in the 2011 Maxar image (Fig. 2) of the World Imagery data) (Fig. 4) were also observed at many of the VRF sites indicating active thermokarst degradation.



165 Figure 2: Maxar (WV02) image of the field region at Mokka Fiord in World Imagery taken in 2011 (Esri, 2018). Seven terraces
containing VRFs are outlined in white. Average elevation (in meters) of each terrace is numbered in white. White dots indicate figure
locations with figure numbers labeled in white. White arrow points to the location of the riverbank in Figure 7a. Elevation contours
are labeled every 50 m and obtained from ArcticDEM Release 7 (Porter et al., 2018). The asterisk elevation denotes the main field
site for in-depth field analysis (i.e., GPR, LiDAR, and trenching). World Imagery Source: Esri, Maxar, GeoEye, Earthstar
170 Geographics, CNES/Airbus DS, USDA, USGS, AeroGRID, IGN, and the GIS User Community.

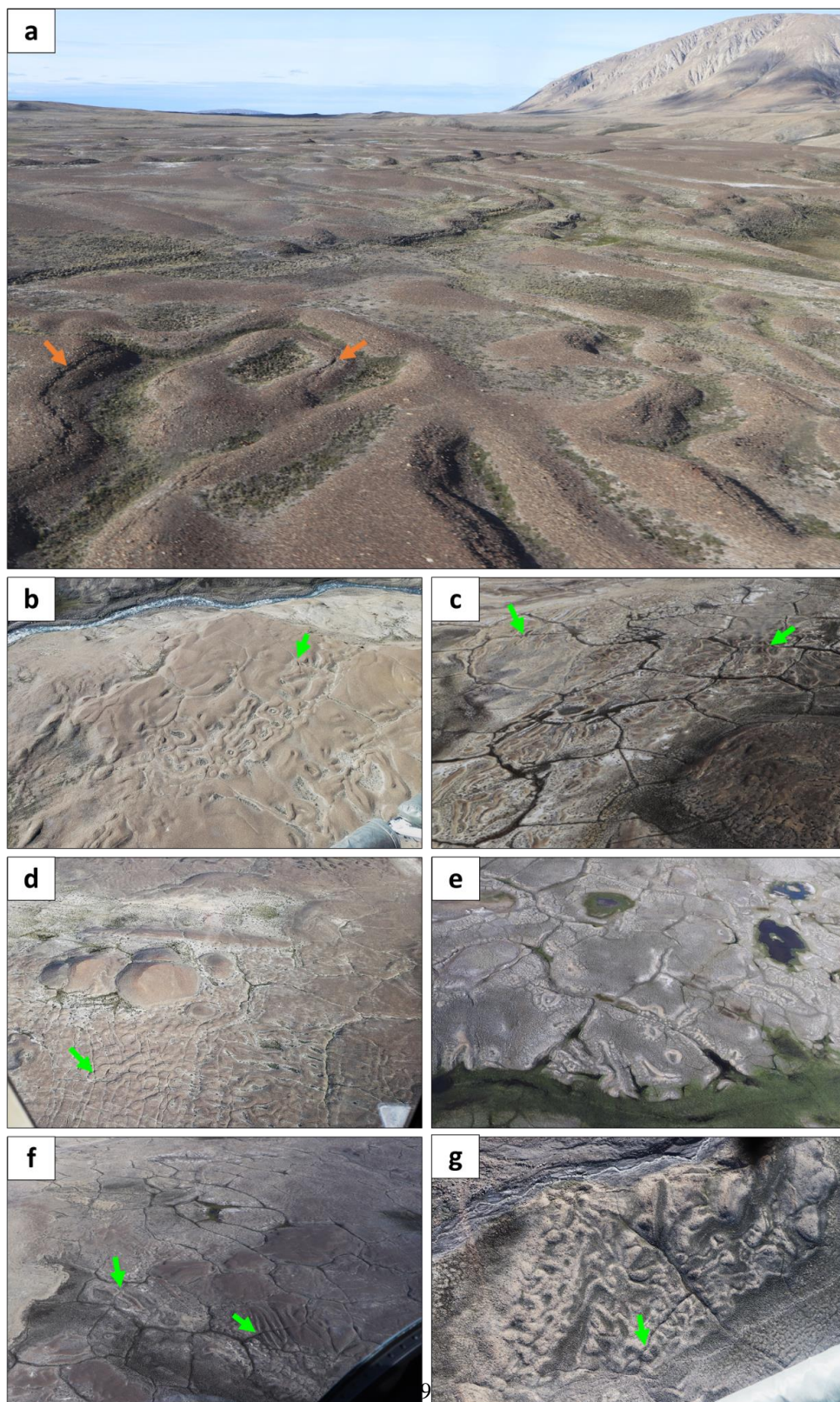


4.2 Morphologic Description of Mokka Fjord VRFs

VRFs found across the field region (Fig. 2) exhibit a circular, elongate, sinuous and/or anastomosing ridge and trough morphology in planform (Figs. 3 and 5). VRFs can create individual closed cells (i.e., ridges creating a closed loop encircling a central trough) that are circular (Figs. 3b, e, and 5), semi-circular (Figs. 3a, b, c, e, and 5) or elongated (Figs. 3c, f, and 5).
175 VRFs range from being closely spaced and interconnected (Figs. 3a, b, d, g) to well-spaced and isolated (Fig. 3e), or somewhere in between (Figs. 3c, f, and 5). Minimal vegetation is found in the field region but can act as a distinguishing factor between the ridges and their surroundings (Figs. 3 and 5b).

One terrace was surveyed in detail (referred to as the main field site) to further investigate the VRFs (Figs. 2 and 5). VRFs at
180 this site have raised convex ridges that stand above the rest of the deposit in which they reside and frequently encircle a central concave depression creating individual closed-cells (Fig. 5). Ridges can also be subdued, shallow and wide relative to the more prominent narrow convex ridges (Fig. 5). Small sharp-crested conical mounds (Fig. 3d) and rounded mounds (Fig. S1a,b, Supp. Files) can be found in the same deposit as VRFs. Terrain adjacent to the ridges and closed cells is referred to as the “mesh” which is the part of the deposit that interconnects VRFs (Fig. 6). The central depressions of closed-cell VRFs lie at the
185 same elevation as or higher than the mesh with the ridges elevated above their adjacent terrain (Figs. 5 and 6). Topographic profiles (Fig. 6) of the VRFs show this mesh-ridge-trough sequence. The topographic lows (e.g., mesh and central depressions) at the main field site are poorly drained and host grasses and mosses (Fig. S1c, d, Supp. Files) compared to the dryer ridges that host lichens (Fig. S2, Supp. Files). A thin white salt crust can also be found across the VRF materials (i.e., the materials of which the ridges, troughs and mesh are composed) (Fig. 5a) generally found resting at the base of the ridges or in topographic
190 lows.

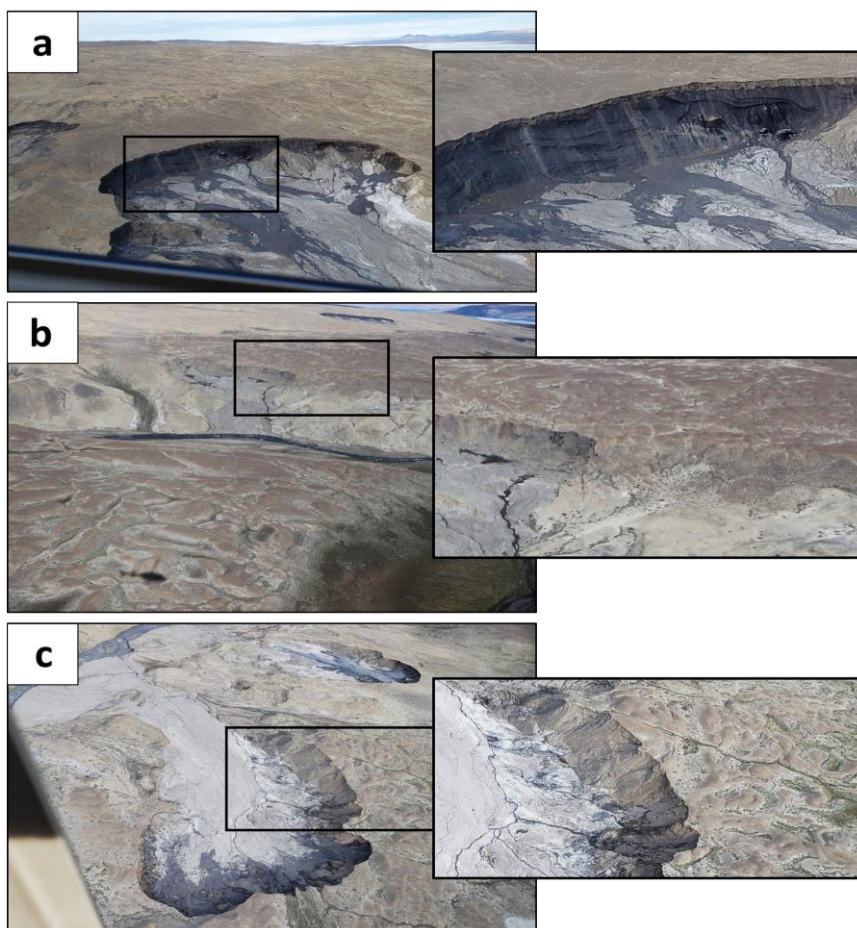
The VRF materials at the main field site are cut by a stream exposing a ~6 m thick cliff that transitions into a ~12 m thick gentler sloping lobate material before connecting with the riverbed (Figs. 2 and 7a), suggesting the deposit has a minimum thickness of ~6 m at the river cutbank relative elevation. A pit was dug 89 cm into the mesh of the deposit without reaching
195 the thaw depth (July 2019) (Fig. 7b). The deposit (observed at the cutbank and in the pit) is a gravelly diamicton composed of poorly sorted, clast-rich, sub-rounded to rounded silt, sand, pebbles and cobbles with minor evidence for a preferred flat orientation of large grains (Fig. 7b). Fewer cobbles were present below 70 cm in the pit. Small pits (~ 10 cm deep) were also dug in a ridge and central trough of a closed-cell VRF. No grain sorting was observed. A fabrics and grain size analysis were not done due to helicopter time constraints at the field site.





205 **Figure 3: Examples of VRFs in the field as seen from a helicopter. Figure locations can be found in Figure 2. Green arrows show where VRFs are cross-cut by polygon troughs. (a) VRFs at the main field site near Mokka Fiord looking north. Mokka Fiord Diapir is in the background to the north. Cracks can be seen along or just off of the axial trace of some of the ridges (orange arrows). (b) VRFs on the terrace on the opposite side of the channel in the field region. (c) VRFs north of the field region, directly west of Mokka Fiord Diapir. (d) Sharp-crested mounds and VRFs south of the field site. (e) Light-toned VRFs north of the field region, west of Mokka Fiord Diapir. (f) Linear VRFs in a dark-toned deposit directly west of Mokka Fiord Diapir. (g) VRFs near Strand Fiord.**

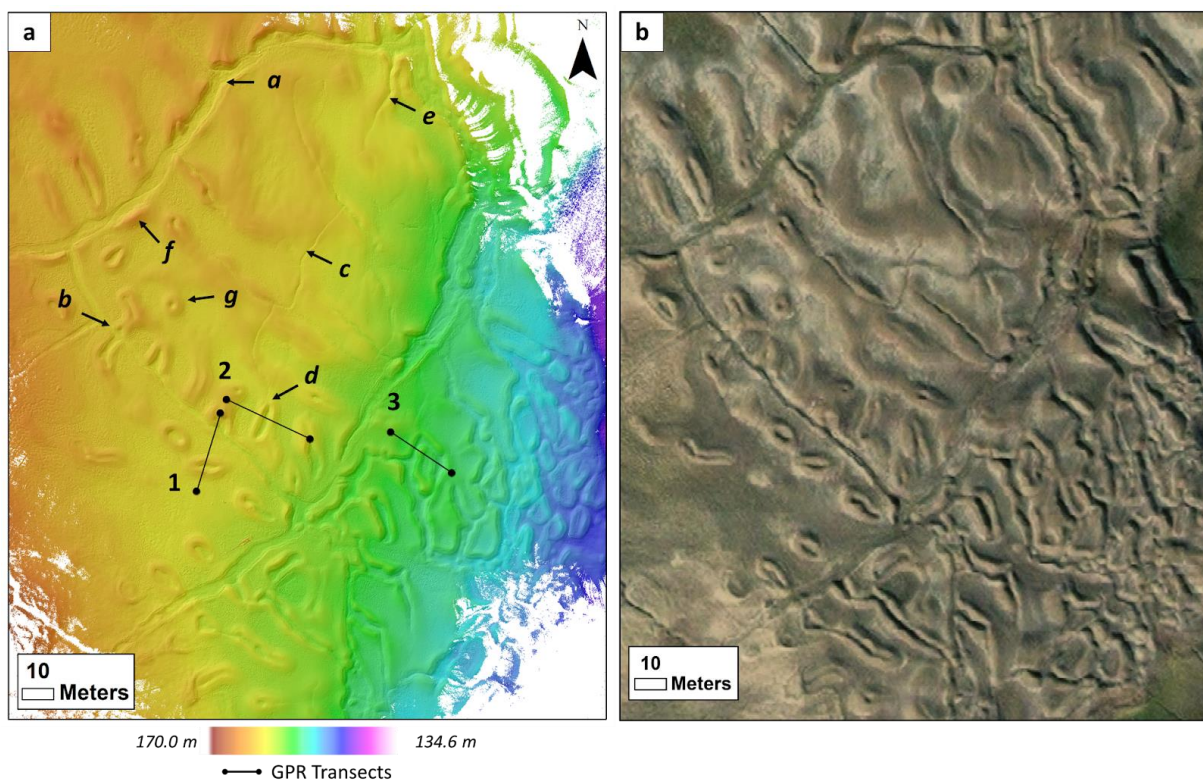
Ridges can reach up to 1.5 m in height when measured from the ridge apex to the adjacent low-lying terrain (i.e., mesh); although most do not exceed 1 m in height (Figs. 5 and 6). Closed-cell ridges (i.e., ridges that enclose a central depression) range in height between 0.2 and 0.6 m when measured from the lowest point in the central trough to the highest point on the ridge (Fig. 6). Ridge width ranges between 1.5 and 9 m but more commonly ranges between 3 and 4 m from the outer edges of the ridge (Fig. 5).



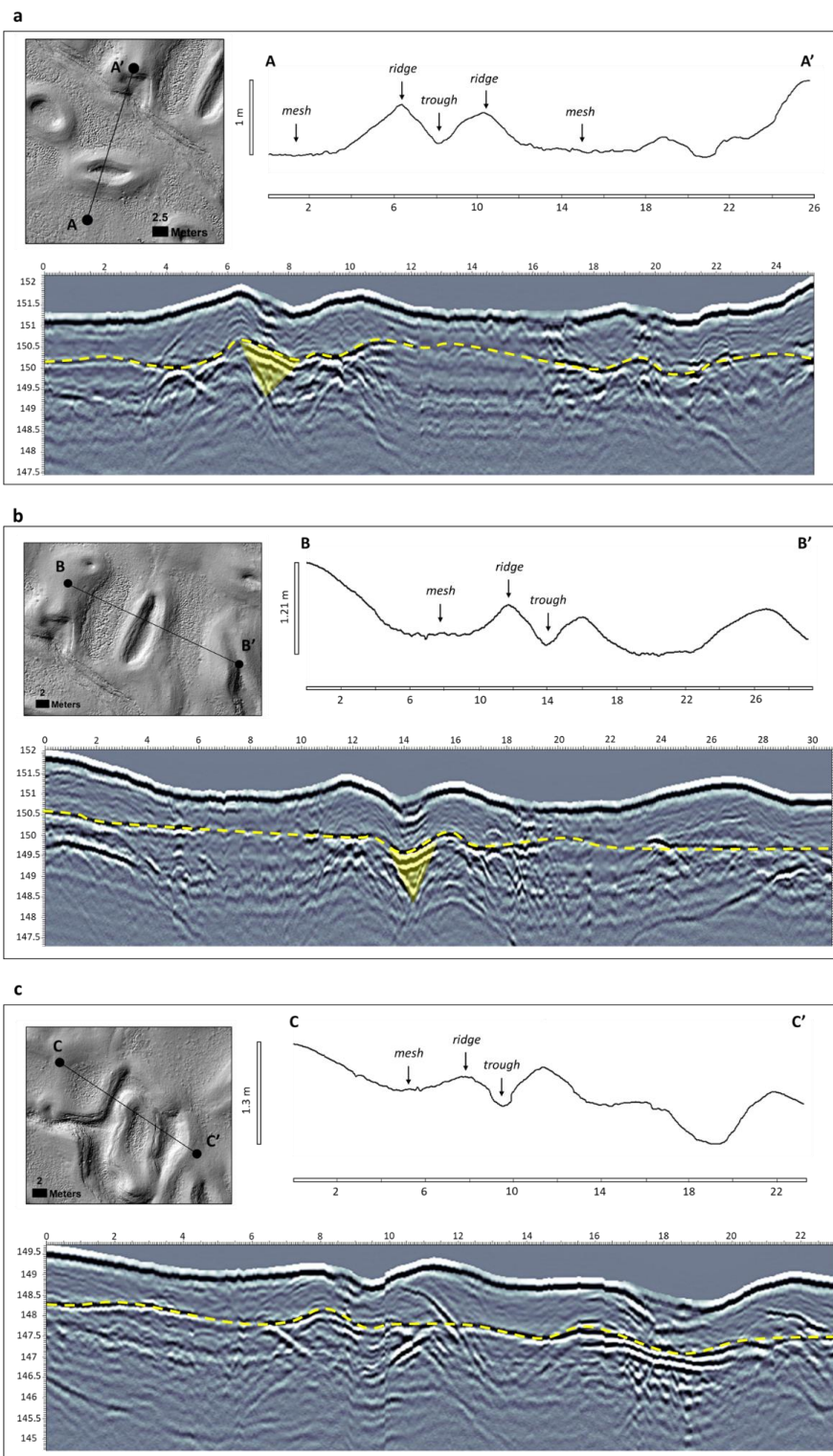
215 **Figure 4: Thaw slumps in the field region. Figure locations can be found in Figure 2 by white dots. (a) West side of channel, south of field site. Possible massive ice exposed at thaw slump. Thaw slump exposure is around 10–15 m thick, including ~1–2 m of dry material above wet material. (b) East side of the channel, directly opposite the field site. A brown deposit with VRFs overlies a lighter-toned deposit. Overlying deposit thickness is around 10–15 m. (c) West side of channel, south of field site. Deposit with VRFs overlies lighter-toned sediments. Deposit thickness is roughly 10–15 m.**



- 220 Thirty-two closed-cell VRFs with central troughs were mapped in the LiDAR area. The long axis of closed-cell ridges ranges between 5.8 and 36.8 m with an average of 15.8 m. The orientation of the long axes (north = 0°) range between 1.8° and 174.5° with an average of 95.7°. This orientation is near perpendicular to the roughly north-south running channel hosting the terraces (Fig. 2). The short axis of closed-cell ridges ranges between 4.3 and 12 m with an average of 8.2 m.
- 225 Cracks were found running along or just off-center from the axial trace of many ridges (Figs. 3a and S2, Supp. Files), and closed-cell ridges generally have a crack running off-center from the axial trace along the inner part of the cell (Fig. S2a, Supp. Files). Cracks present themselves as a thin and narrow cavity along the ridge (Figs. 6 and S2, Supp. Files), and slumping of the surrounding material may be present. Cracking also occurs along the center of polygon troughs and along the shoulders of polygons (Fig. S2c, Supp. Files), both of which tend to be much wider (≤ 30 cm) and deeper than the cracks observed on the
- 230 ridges of VRFs.



235 **Figure 5: Digital Elevation Model of VRFs at the main field site. (a) DEM is overlying hillshade with 315° azimuth. GPR transects 1–3 are numbered and outlined in black. Topographic profiles and GPR transects can be found in Figure 6. Features of note include: a shallow and wide raised ridges cross-cut by polygon trough, b closed-cell VRF cross-cut by polygon trough, c secondary trough cross-cutting VRFs, d secondary trough cuts down through the middle of a closed-cell VRF, e secondary trough runs down the middle of a shallow sinuous VRF, f raised polygon shoulder, g perfectly circular individual closed-cell VRF. (b) Main field site LiDAR area in World Imagery (Esri, 2018). World Imagery Source: Esri, Maxar, GeoEye, Earthstar Geographics, CNES/Airbus DS, USDA, USGS, AeroGRID, IGN, and the GIS User Community.**

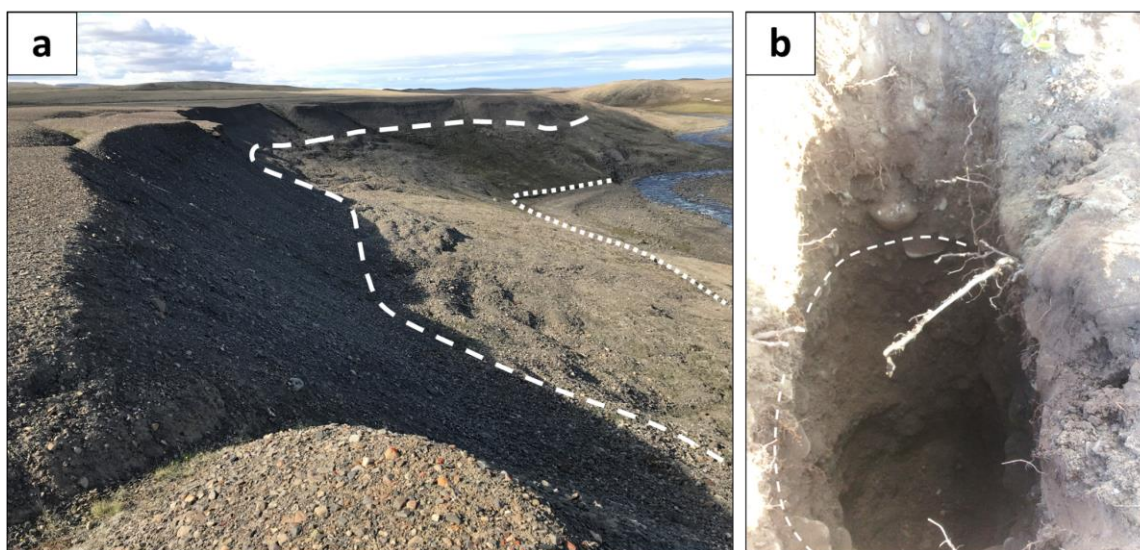




240 **Figure 6: LiDAR Hillshade, LiDAR-derived topographic profiles and GPR transects of VRFs. Transect locations can be found in**
Figure 5. Units in meters. Maximum vertical relief on the y-axis of topographic profiles. Elevation is on the y-axis of GPR
transects. (a) Line 1 (A-A'), (b) Line 2 (B-B') and (c) Line 3 (C-C') topographic profiles demonstrate a mesh-ridge-trough
sequence. VRF troughs are pointed to bowl-shaped concave depressions. Yellow dashed line in GPR transects represents thaw
depth (i.e., depth to permafrost in July 2019). Bright reflectors can be seen beneath closed cell VRF central troughs indicating the
245 **presence of ice. These reflectors demonstrate a wedge-shaped object (shaded in yellow) in Lines 1 and 2.**

Well-developed polygons are also present at the main field site. Polygons range in diameter (long axis) between 115 and 167
m, and trough width averages around 3 m, but can reach up to nearly 6 m. Thin and narrow secondary troughs are present
within the larger polygon centers (Fig. 5). Secondary troughs propagate from a major trough and often terminate within the
250 polygon center (Fig. 5). Polygon troughs appear to typically cross-cut VRFs but can also merge with VRFs to create an
anastomosing ensemble of ridges and troughs (Figs. 3 and 5).

VRF morphology varies laterally and with elevation among the terraces. The main field site is characterized by more mounds
down valley (Fig. S1a, Supp. Files) and less mounds with high-center polygons exposing the VRF-containing deposit up valley
255 (Fig. S1d, Supp. Files). Additionally, the uppermost terrace has a thin VRF-containing deposit that appears degraded (i.e.,
subtle hummocks, thin deposit, less pronounced morphology) (Fig. S1e, Supp. Files) relative to VRFs on neighboring, lower
terraces that appear to reside in much thicker deposits (Fig. S1b,f, Supp. Files). Additionally, more vegetation is present at the
main field site (Fig. S1c,d, Supp. Files) compared to the other terraces (e.g., Fig. S1a,b,e,f, Supp. Files).



260 **Figure 7: Characteristics of VRF materials at river cutbank. (a) River cutbank exposing deposit thickness (Location identified in**
Figure 2). Polygons are visible at the top of the deposit. The surface to the white dashed line is characterized by a steep talus slope ~
6 m thick. A gently sloped section of lobate material occurs between the white dashed line and the white dotted line. Below the white
dotted line is a river sand bank. (b) Pit dug 89 cm into the main field terrace. White dashed line outlines flat-oriented gravel.



265 Three GPR transects were collected at the main field site. Lines 1, 2, and 3 cross over closed-cell VRFs (Figs. 5 and 6) and
show a thaw depth (July 2019) ranging between 1 and 1.5 m that can be identified by a nearly continuous bright linear reflection
below the surface (Fig. 6). Stacked bright radar reflections are observed below the central depression of a close-cell ridge at
Lines 1 and 2 (Fig. 6). Line 3 shows bright reflections beneath two troughs adjacent to a closed-cell ridge. However, the center
of the closed-cell ridge at Line 3 does not appear to have an obvious bright reflection. Deposit thickness is indeterminate in
270 the GPR transects, suggesting the deposit thickness exceeds the signal penetration depth of approximately 4 m. VRFs were
also observed directly on top of thaw slumps across the field region, which exposed deposits as thick as 10 to 15 m.

5 Discussion

We have documented an unusual landform, referred to here as Vermicular Ridge Features (VRFs), northwest of Mokka Fiord
on Axel Heiberg Island, Nunavut, Canada. These features exhibit a circular, elongated, sinuous, and/or anastomosing series of
275 ridges and troughs (Figs. 3 and 5). Below, we compare VRFs on Axel Heiberg Island to other morphologically similar
periglacial and glacial landforms, namely lithalsas and morainic rim ridges, in order to better elucidate an origin (Table 1).

5.1 Periglacial Origins

Patterned ground is a common product of periglacial processes that can result in conspicuous morphologies such as circular,
280 sinuous, and anastomosing ridges and troughs. Stone circles are a common periglacial feature that exhibit this morphology and
can be found in high and low Arctic regions (Washburn, 1956; Schmertmann and Taylor, 1965; Washburn, 1973; Hallet and
Prestrud, 1986; Hallet, 2013). Stone circles are characterized by their circular to labyrinthine coarse-grained ridges surrounding
a central fine-grained domain. Ridge width typically ranges between 0.5–1 m and ridge height usually reaches up to 0.5 m,
with circle diameters ranging between 2–5 m (Hallet and Prestrud, 1986; Kessler et al., 2001; Hallet, 2013). Stone circles also
285 commonly exhibit cracks along the axial trace of circular ridges that form from frost heave and soil upwelling (Kääb et al.,
2014). However, while the scale is similar, no grain sorting or evidence of soil upwelling was observed in the Mokka Fjord
VRFs and the microtopography does not reflect that of stone circles. Thus, the properties of the Mokka Fjord VRFs are
inconsistent with being stone circles.

290 Collapsed pingos, palsas, and lithalsas (Table 1), also referred to as circular ramparts or ramparted depressions, and other frost
mounds and blisters are periglacial landforms that can also result in circular raised ridge features (Table 1) (Mackay, 1998 and
references therein). Pingos are perennial ice-cored hills produced by injection of groundwater under artesian pressure (Holmes
et al., 1968; Müller, 1962) or by pore-water expulsion resulting from permafrost aggradation in a water-saturated sandy
sediment, such as a shallow lake (Mackay, 1998). Pingos are much larger in scale and typically occur singularly (Table 1) and,
295 therefore, are not an explanation for the VRFs at Mokka Fjord.



Table 1: Periglacial and glacial ring ridge feature morphometrics compared to Mokka Fjord VRFs. Modified from Hibbard et al. (2021).

Name	Location	Age of Formation (ka BP)	Diameter	Height	Ridge Material	Formation Mechanism	Reference
<i>This study</i>							
Vermicular Ridge Features (VRFs)							
	Axel Heberg Island, Nuнавut, Canada	≤ 10	6–37 m	up to 1.5 m	clast-rich sandy glaciofluvial sediment and till	ice-marginal glaciofluvial and supraglacial origin, dead ice ablation	This study
Periglacial in Origin							
Peiljavani rim ridges	northern Finland	< 9–10	30–150 m	0.5–4.5 m	unstratified poorly sorted sandy till	collapsed open system pingo-like front mounds (i.e., lithalis)	Seppälä, 1972
Circular lakes	northern Norway	> 1.3	up to 40 m	up to 1.5 m	fine-grained glaciofluvial deposits with peat lenses	collapsed minerogenic front mounds (i.e., lithalis)	Svensson, 1969
Ground ice depressions	East Anglia, UK	11	10–120 m	up to 3 m	fine chalk rubble and sand with thin organic lenses	collapsed front mound thermokarst degradation	Sparks et al., 1972
Remains of pingos	Southwest Wales, UK	–	60–165 m	can exceed 10 m	clay silt and gravelly clay	collapsed open system pingos	Watson and Watson, 1974 (same feature described by Ross et al., 2019)
Palsa-like mounds	northern Sweden	–	4–40 m	1–2 m	silty/clayey material with a high block content to blocky only	collapsed palsa-like front mounds	Åkerman and Malmström 1986; Rapp and Rusbberg, 1960
Palaeo thermokarst depressions	South Bohemia, Czech Republic	14–16	up to 120 m	up to 6 m	sandy gravel	collapsed lithalis subsequently filled with lake basin sediments	Hošek et al., 2019
Visvers-lithala remnants	eastern Belgium	11–12	up to 250 m	< 1 m, up to 8 m	clayey silt with pebbles and peat	collapsed lithalis	Pisart, 2003 and references therein
Pingo lithalis remnants	southern Ireland	10–11	50–100 m	1–2 m	course sand and frost-shattered pebbles	collapsed lithalis	Coxon, 1986; Coxon and O'Callaghan, 1987; Pisart, 2003
Decayed lithalis	Umanjag, Nunavut, Northern Quebec	0.1–1.5	50 m	2–3 m	silt and clay layer overlying sand and gravel layer	eroded palsa, now lithalis at initial stage of degradation/collapse	Caineli et al., 2008
Ice-cored depression	southern Netherlands	~14–18	up to 90 m	3 m	sandy material	collapsed pingo lithalis	Kasse and Bolincke, 1992
Lithalis	Northwest Territories, Canada	0.7	10–120 m	0.5–8 m	silt, clay, and sand	degraded and collapsed lithalis	Wolfe et al., 2014
Glacial in Origin							
Ring ridge moraines	Devon Island, Nunavut, Canada	< 8	4–72 m	up to 2.5 m	clast-rich sandy till	supraglacial origin, dead ice ablation	Hibbard et al., 2021
Hummocky terrain	north-central Alberta, Canada	11–13	–	2–10 m	sandy silt/silty clay with 5–10% clast till	subglacial squeezing	Paulsen and McCreaghghan, 2014
Pulju Moraines	Finland	9–10	30–100 m	< 1.5 m; 1.6–2.1 m	gravelly to sandy and silty till	subglacial squeezing	Sunmaa et al., 2014
Circular Ridges	Norway	~14	50–100 m	2.5–10 m	clast-rich sandy till	supraglacial origin, dead ice ablation	Kundsen et al., 2006
Rampoured Depressions	Wales	–	60–165 m	can exceed 10 m	clayey silt and occasional clasts - glacial distinct and glaciolacustrine sediments	either supraglacial or subglacial	Ross et al., 2019 (same feature described by Watson and Watson, 1974)
Veali Moraines	Sweden	< 11–12	100s of m	6–10 m	clay, silt, sand, gravel	subglacial and supraglacial origins	Lagerbäck, 1988
Ring Ridge Hummocky moraines	northern Finland	–	20–200 m	0.5–4 m	sandy silty till with some gravel and with boulders on ridges overlying clay-rich till	supraglacial origin, dead ice ablation	Aströhm, 1974
Ice-Contact Rings	Saskatchewan, Canada	–	10s of m	1.5–10.5 m	till, sand and gravel	supraglacial origin, dead ice ablation	Pattsek, 1969
Rogen Moraine	Sweden	–	up to 100 m	up to 30 m	laminated tills with interbedded sorted sediments (Kaibe till and Sveg till)	supraglacial origin, dead ice ablation	Lundqvist, 1989
Circular moraine features (CMF)	northern Norway	11–15	20–170 m	0.5–10 m	diamicton	englacial origin; dead ice ablation	Ebert and Kleman, 2004



Lithalsas are smaller scale frost mounds that form by ice segregation in mineral-rich soil absent of peat and can be found on river terraces and along streams. They form through permafrost aggradation causing localized ice segregation as pore water migrates (Calmels et al., 2008). The formation of lithalsas requires specific environmental conditions in order to allow slow freezing times to promote cryosuction for ice lense growth. The limited examples of contemporary lithalsas appear to be restricted to the discontinuous permafrost zone with available groundwater supply and in frost susceptible fine-grained sediment as opposed to the coarser grained till present in our study area (Calmels et al., 2008; Wolfe et al., 2014); although others have proposed lithalsa remnants to be present in coarse-grained materials (e.g., Seppala, 1972; Akerman and Malmstrom, 1986; Rapp and Rudberg, 1960; Hosek et al., 2019; Coxen, 1986). More importantly, Mokka Fjord VRFs are located in the continuous permafrost zone and have been in a polythermal and cold glacial environment with little water supply since the retreat of the Innuitian Ice Sheet (Ó Cofaigh et al., 1999). Therefore, the strict environmental conditions necessary for lithalsa formation would not have been met at Mokka Fjord. Furthermore, VRFs at Mokka Fjord exhibit a much more complex morphology than has been observed in remnant and contemporary lithalsas (Fig. 3), which tend to be circular ramparts.

Other segregation ice landforms, such as the Involute Hill sites located in Tuktoyaktuk, Northwest Territories, Canada, exhibit a similar, yet not identical, complex morphology as observed in Mokka Fjord VRFs. The Involute Hills are clay till-mantled ice-cored hills with a series of ridges and troughs. The ridges there are approximately 10 to 40 m wide, several tens of meters in length, and up to 6 m in height, which is much larger than the Mokka Fjord VRFs (Mackay, 1963; Rampton, 1988; Mackay and Dallimore, 1992). Mackay and Dallimore (1992) suggest glacial meltwater and porewater expulsion are what led to the formation of the massive ice at Involute Hill, and that differential degradation of that ice led to the series of ridges and troughs at the surface. While it may be possible that the Mokka Fjord VRFs formed as localized frost mounds or other segregation ice mounds, we consider it highly unlikely due to the limited water supply from polythermal glaciers.

Smaller pingo-like frost mounds and partially collapsed mounds have been documented in the Canadian High Arctic on Banks Island, Northwest Territories, and suggested to form from the freezing of fluvial taliks left over from previous lateral stream migration (Pissart and French, 1976, 1977). Additionally, pingos in Svalbard have been suggested to form from the infiltration and migration of polythermal glacial meltwater to taliks (Liestøl, 1977). Mokka Fjord VRFs occur within a fluvial/glacio-fluvial setting that has sediments conducive to the upward and lateral movement of groundwater. Therefore, Mokka Fjord VRFs could have formed from the freezing of glacial meltwater taliks in fluvial/glacio-fluvial sediments and/or till due to permafrost aggradation following glacial retreat. This would then be followed by differential ablation leading to the formation of a series of ridges and troughs.

Although we have not entirely ruled out periglacial origins, Axel Heiberg Island lies within a recently deglaciated landscape where large amounts of dead glacial ice are likely preserved in the continuous permafrost zone under the protection of surface



debris cover. Morphologically similar features can form from the ablation of buried glacial ice as well as from other glacial-related processes. Therefore, we consider possible glacial formation mechanisms and analogous landforms to compare to Mokka Fjord VRFs.

335 5.2 Glacial Origins

Ring ridge moraines (a general term used to encompass the variety of naming schemes used in the literature) are glacially derived circular to anastomosing raised ridge features found largely across northern Europe and North America (Table 1). Although ring ridge moraine origins remain debated, their formation is largely attributed to one of the following two main hypotheses: (1) supraglacial and englacial debris concentrations left over from the disintegration of stagnant proglacial/ice-
340 marginal ice, including Circular Ridges in Norway (Knudsen et al., 2006), VRFs on Devon Island in Nunavut, Canada (Hibbard et al., 2021), Veiki Moraines in Sweden (Lagerbäck, 1988), Pulju Moraines in northern Finland (Aartolahti, 1974; Sutinen et al., 2014, 2018, 2019; Middleton et al., 2020), and Ice-Contact Rings in Saskatchewan, Canada (Lundqvist, 1989), or (2) subglacial diapirism and the filling of subglacial cavities with basal water-saturated till that leaves behind ring ridges after the
345 Moraines in Finland (Sutinen et al., 2014), Rogen Moraines in Sweden (Lundqvist, 1989), and Circular Moraine Features in northern Norway (Ebert and Kleman, 2004). More details regarding the various types ring ridge moraines and their specific differences are described in Johnson and Clayton (2005) and Hibbard et al. (2021).

There is considerable variation in the scale, landform association, and sedimentology of ring ridges (Table 1), yet many are
350 found in farmland and vegetated regions, which likely leads to the preferential preservation of large-scale landforms, and only a handful are comprised of coarse-grained sediment (Table 1). Mokka Fjord VRFs are small-scale and occur in coarse-grained sediments. Additionally, the morphometry, affiliated ice sheet characteristics, and thermal regime (i.e., Innuitian, Laurentide, Celtic, and Fennoscandian Ice Sheets), and/or deposit age of ring-ridge moraines differ markedly from the Mokka Fjord VRFs (Table 1). Only the Dundas Harbour ring-ridge moraines (Hibbard et al., 2021) are comparable in both morphometry and
355 sedimentology to Mokka Fjord VRFs among other coarse-grained glacially derived ring ridges (Table 1).

Ring ridges at Dundas Harbour (Hibbard et al., 2021) are identical in morphology and morphometry to the VRFs at Mokka Fjord. For example, individual circular closed-cell VRFs on Dundas Harbour (Devon Island) and Mokka Fjord (Axel Heiberg Island) exhibit an identical microtopography consisting of rounded convex ridges, a u-shaped concave central depression with
360 an abrupt change in slope at the ridge-trough transition, miniature grooves where cracks along the ridge apex occur, and gradual outward-facing slopes leading to the mesh (Fig. 8). The sedimentology of ring ridges at Dundas Harbour was interpreted as a sandy clast-rich till based on grain size analyses (Hibbard et al., 2021). Although no grain size distribution was done on Mokka Fjord VRFs, extensive field observations indicate the material is composed of sub-rounded clast-rich sand and shows minor

evidence of preferred orientation and minimal stratification of sands and gravels in the pits dug and exposures observed in the
365 field. The sedimentology at Mokka Fjord is most consistent with a glaciofluvial deposit rather than a glacial till.

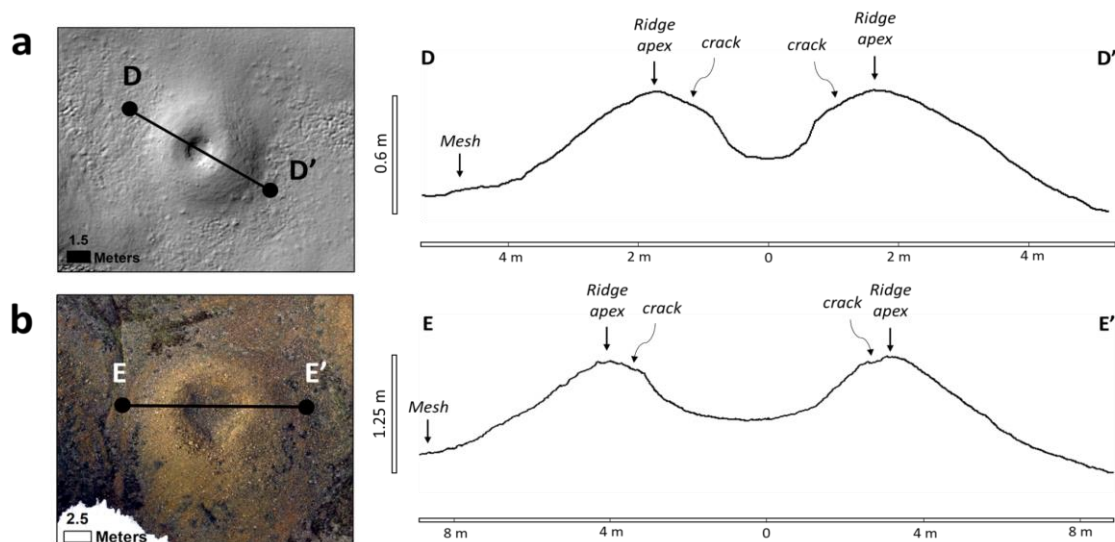


Figure 8: Topographic profiles of circular closed cell VRFs at Mokka Fiord and Dundas Harbour. (a) Example of circular VRF at Mokka Fiord, Axel Heiberg Island, Nunavut, Canada (D-D'). LiDAR data on the left and topographic profile on the right. VRF displays rounded convex ridges with cracks running just off the axial trace of the ridge, a u-shaped central trough following an abrupt change of slope from the ridge cracks, and a gently sloping transition into the mesh. (b) Example of circular VRF at Dundas Harbour on Devon Island, Nunavut, Canada (E-E'). Aerial drone imagery on the left and topographic profile on the right. VRF displays the same microtopography observed in (a) with a larger diameter. Modified from Hibbard et al. (2021).

It is notable that thermal contraction crack polygons are observed at Mokka Fiord and clearly cross-cut the VRFs indicating post-depositional modification of the VRF materials (Figs. 3, 5, S1, Supp. Files). This relationship is also observed at Dundas
375 Harbour (Hibbard et al., 2021). However, polygons at the main Mokka Fiord field site are much more developed and well defined compared to those at Dundas Harbour. For example, the polygon troughs are wider, have raised shoulders with cracks running parallel to the troughs, and have both primary and secondary troughs with ice wedges. In addition to ice-wedge polygons, Mokka Fiord has exposed ice at active thaw slumps; whereas no evidence for massive buried ice was observed at Dundas Harbour. This may be the product of more ice (and therefore more water) in the region and longer subaerial exposure
380 at Mokka Fiord as the field site is much farther away from the ice caps compared to the ring ridges located at Dundas Harbour (Hibbard et al., 2021). Therefore, despite their identical morphology and morphometry, the depositional environment was different at Mokka Fjord and Dundas Harbour. Which begs the question, are ring ridges at Dundas Harbour the same as VRFs at Mokka Fjord or are their similarities a product of equifinality suggesting that different processes can lead to a similar geomorphic expression? And, if so, what are the processes involved?

385 Bednarski (1998) describes the Quaternary geomorphology and stratigraphy of northeastern Axel Heiberg Island, which is ~300 km northeast of our field site at Mokka Fiord and lies within the outwash plains emanating from the Princess Margaret



Range. The outwash plains described by Bednarski (1998) are reported to host extensive kettled outwash terraces (an ice-marginal or distal proglacial landform, and kame terraces (an ice-marginal glacial landform).

390 The kettled outwash/kame terraces described by Bednarski (1998) are reported to be composed of ice-contact glaciofluvial coarse gravel with kettles and kames that range from 30–50 m in relief, ice-contact ridges, and active slumping that indicates the presence of buried glacial ice. Kame terraces are also suggested to be present along the west coast of Flat Sound (Fig. 1) where a northwest-flowing trunk glacier in Nansen Sound was in contact with the eastward-flowing glaciers from the Axel highlands (Bednarski, 1998).

395

Land-based ice on Axel Heiberg Island deglaciated between 9 and 7.5 ka BP (England et al., 2006). If Mokka Fjord VRFs were to have formed from frost mounds, massive segregated ice near the coast, as well as the formation of terraces and the differential ablation of buried ice to form VRF ridges, would need to have formed in less than 1,500 years. Massive intrasedimental ice has been identified in northern Canada, as well as on Axel Heiberg Island, but is typically found in fine-grained marine or glacial lake sediments below the marine limit (e.g., Pollard, 2000; Roy et al., 2018) as a result of permafrost aggradation following glacio-isostatic emergence (Pollard and Bell 1998). Mokka Fjord VRFs are not in marine sediments and the field site is at the upper limit or above the Holocene marine limit range. The terraces are comprised of glaciofluvial deposits and landforms that resemble kames, dead ice disintegration features, and possible eskers, all of which would be expected in a glaciofluvial/ice-marginal setting (e.g., King and Buckley, 1969; McKenzie and Goodwin, 1987).

405

Therefore, we suggest that the Mokka Fjord VRFs most likely formed from the burial and eventual detachment of ice-marginal/snout glacial ice followed by differential ablation of ice leading to a series of ridges and troughs as was suggested for VRFs at Dundas Harbour (Hibbard et al., 2021).

6 Summary and Conclusions

410 Vermicular Ridge Features (VRFs) at Mokka Fjord exhibit a circular, elongated, sinuous, and/or anastomosing morphology as a series of ridges and troughs. They occur along terraces and within the floodplain of a glacial meltwater channel. Thaw slumps (Fig. 4), active lobate slumping (Fig. 7), and thermokarst degradation (Fig. 3e) found among the VRFs suggest the presence of buried massive ice underneath. However, the origin of this ice is not known.

415 The leading periglacial (i.e., segregation ice features/lithalsas) and glacial (i.e., ring-ridge moraines and kame/kettled terraces) origins discussed above for Mokka Fjord VRFs all involve buried massive ice and the differential ablation of that ice to form the resulting surface topography and morphology. As the ice melts, the overlying deposit redistributes to preferentially promote a hummocky surface, like the process described by Hibbard et al. (2021) for identical features on Devon Island. Hence, the process of debris-mantled ice disintegration can form morphologically similar features regardless of the exact mechanism of



420 debris transport and deposition needed prior to VRF formation, and regardless of the ice origin. This presents the ongoing difficulty in distinguishing periglacial and glacial landforms in ice-cored terrain that result in a near identical morphology (e.g., Rampton, 2001; Ross et al., 2019; Dyke and Evans, 2003), and, consequently, the concept of equifinality in geomorphology (e.g., Haines-Young and Petch, 1983; Möller and Dowling, 2018).

425 Based on our observations, we interpret Mokka Fjord VRFs to be an ice-marginal feature resulting from paraglacial ablation of buried glacial ice producing a hummocky ring-ridge moraine comprised of supra- and englacial debris. This formation mechanism would infer a largely polythermal glacial environment with limited water supply. Likely from occasional warm-based periods at the ice margins which may allow sediment output and ice burial from basal ice debris redistribution or the thinning and subsequent burial of snout ice from glaciofluvial outwash.

430 **Competing Interests**

The contact author has declared that none of the authors have any competing interests.

Acknowledgements

We would like to thank the Inuit of the Qikiqtani Region (one of the three regions in the territory of Nunavut). Fieldwork was carried out on their land in Nunavut. We would like to thank the community of Qausuittuq (Resolute Bay) for welcoming us
435 during our stay in the summer of 2019. Logistical support from the Polar Continental Shelf Program (NRCan) is gratefully acknowledged. Funding was provided by a Canadian Space Agency (CSA) Flights and Fieldwork for the Advancement of Science and Technology (FAST) grant and Natural Sciences and Engineering Research Council of Canada (NSERC) Discovery Grant Northern Supplement to GRO. SH was supported by an appointment to the NASA Postdoctoral Program at the Jet Propulsion Laboratory, California Institute of Technology, administered by Oak Ridge Associated Universities under
440 a contract with NASA (80HQTR21CA005). The research was carried out at the Jet Propulsion Laboratory, California Institute of Technology, under a contract with the National Aeronautics and Space Administration (80NM0018D0004). Reference herein to any specific commercial product, process, or service by trade name, trademark, manufacturer, or otherwise, does not constitute or imply its endorsement by the United States Government or the Jet Propulsion Laboratory, California Institute of Technology. The authors would like to thank Academy of Finland (Coe-LaSR, MS-PLS 300066) and Strategic Research
445 Council at the Academy of Finland project "Competence Based Growth Through Integrated Disruptive Technologies of 3D Digitalization, Robotics, Geospatial Information and Image Processing/Computing - Point Cloud Ecosystem (293389/314312)." Geospatial support for this work provided by the Polar Geospatial Center under NSF-OPP awards 1043681 and 1559691 allowed for the use of ArcticDEM data for this project. Figures throughout this article were created using ArcGIS® software by Esri. ArcGIS® and ArcMap™ are the intellectual property of Esri and are used herein under license.



450 Copyright © Esri. All rights reserved. For more information about Esri® software, please visit www.esri.com. We would also like to thank Inuit Tapiriit Kanatami for their map of Inuit Nunangat, which was used for referencing Inuktitut geographical terms.

References

- Aartolahti, T.: Ring ridge hummocky moraines in northern Finland, Fenn. - Int. J. Geogr. 134, 1974.
- 455 Andersen, D.T., Pollard, W.H., McKay, C.P., Heldmann, J.: Cold springs in permafrost on Earth and Mars, J. Geophys. Res. E Planets 107, 4–1. <https://doi.org/10.1029/2000je001436>, 2002.
- Balkwill, H.R.: Evolution of Sverdrup Basin, Arctic Canada, AAPG Bull. (American Assoc. Pet. Geol. 62, 1004–1028.
- 460 <https://doi.org/10.1306/c1ea4f86-16c9-11d7-8645000102c1865d>, 1978.
- Bednarski, J.M.: Quaternary history of Axel Heiberg Island bordering Nansen Sound, Northwest Territories, emphasizing the last glacial maximum, Can. J. Earth Sci. 35, 520–533. <https://doi.org/10.1139/e97-124>, 1998.
- 465 Blatter, H.: On the thermal regime of an Arctic valley glacier: a study of White Glacier, Axel Heiberg Island, NWT, Canada, Journal of Glaciology, 33, 114, 200–211. <https://doi.org/10.3189/S0022143000008704>, 1987.
- Calmels, F., Allard, M. and Delisle, G.: Development and decay of a lithalsa in Northern Quebec: a geomorphological history, Geomorphology, 97(3-4), p. 287-299. <https://doi.org/10.1016/j.geomorph.2007.08.013>, 2008.
- 470 Clayton, L.: Karst Topography on Stagnant Glaciers, Journal of Glaciology, 5, 37, 107–112. <https://doi.org/10.3189/S0022143000028628>, 1964.
- Constable, A.J., Harper, S., Dawson, J., Mustonen, T., Piepenburg, D., Rost, B., Bokhorst, S., Boike, J., Cunsolo, A., Derksen, C. and Feodoroff, P.: Climate change 2022: Impacts, adaptation and vulnerability: Cross-chapter paper 6: Polar regions, 2022.
- 475 Dyke, A.S., Dredge, L.A., Hodgson, D.A.: North America deglacial marine- and lake-limit surfaces, in: Géographie Physique et Quaternaire. Presses de l'Université de Montréal, pp. 155–185. <https://doi.org/10.7202/014753ar>, 2005.
- 480 Dyke, A.S. and Evans, D.J.: Ice-marginal terrestrial landsystems: northern Laurentide and Innuitian ice sheet margins. In: Glacial landsystems, Arnold, London, 143–165, 2003.



- 485 Ebert, K., Kleman, J.: Circular moraine features on the Varanger Peninsula, northern Norway, and their possible relation to polythermal ice sheet coverage. *Geomorphology* 62, 159–168. <https://doi.org/10.1016/j.geomorph.2004.02.009>, 2004.
- Embleton, C., King, C. A. M.: *Glacial geomorphology*. Edward Arnold Publishers Ltd. London, UK, 1975.
- Embry, A., Beauchamp, B.: Chapter 13 Sverdrup Basin, in: *Sedimentary Basins of the World*. Elsevier, pp. 451–471. [https://doi.org/10.1016/S1874-5997\(08\)00013-0](https://doi.org/10.1016/S1874-5997(08)00013-0), 2008.
- 490 England, J., Atkinson, N., Bednarski, J., Dyke, A.S., Hodgson, D.A., Ó Cofaigh, C.: The Inuitian Ice Sheet: configuration, dynamics and chronology. *Quat. Sci. Rev.* 25, 689–703. <https://doi.org/10.1016/j.quascirev.2005.08.007>, 2006.
- Environment Canada: Canadian Climate Normals 1981–2010 Station Data. Eureka A station, Nunavut. Government of
495 Canada. http://climate.weather.gc.ca/climate_normals/ (accessed 12 June 2021), 2021.
- Esri: "Imagery" [basemap]. Scale Not Given. "World Imagery". July 18, 2018. <https://www.arcgis.com/home/item.html?id=10df2279f9684e4a9f6a7f08febac2a9>. (accessed 20 June 2020), 2018.
- 500 Fairbridge, R.W.: Inversion (of topography, relief). In: *Geomorphology. Encyclopedia of Earth Science*. Springer, Berlin, Heidelberg. https://doi.org/10.1007/3-540-31060-6_193, 1968.
- French, H.M. and Harry, D.G.: Observations on buried glacier ice and massive segregated ice, western Arctic coast, Canada. *Permafrost and Periglacial Processes*, 1, 1, 31-43. <https://doi.org/10.1002/ppp.3430010105>, 1990.
- 505 Geological Survey of Canada: Surficial geology, western Fosheim Peninsula and eastern Axel Heiberg Island, Nunavut, NTS 49-G and 340-B southwest; Geological Survey of Canada, Canadian Geoscience Map 392 (Surficial Data Model v.2.3.14 conversion of Open File 501), scale 1:125 000. <https://doi.org/10.4095/313535>, 2022.
- 510 Gravenor, C.P., Kupsch, W.O.: Ice-Disintegration Features in Western Canada. *J. Geol.* 67, 48–64. <https://doi.org/10.1086/626557>, 1959.
- Haines-Young, R.H., Petch., R.J.: Multiple working hypotheses: equifinality and the study of landforms. *Trans. Inst. Br. Geogr.* 8 (4), 458–466. <https://doi.org/10.2307/621962>, 1983.



- Hallet, B.: Stone circles: Form and soil kinematics. *Philosophical Transactions of the Royal Society of London. Series A: Mathematical, Physical, and Engineering Sciences*, 371, 2004, 20120357–20120357. <https://doi.org/10.1098/rsta.2012.0357>, 2013.
- 520 Hallet, B., Prestrud, S.: Dynamics of periglacial sorted circles in western Spitsbergen. *Quat. Res.* 26 (1), 81–99. [https://doi.org/10.1016/0033-5894\(86\)90085-2](https://doi.org/10.1016/0033-5894(86)90085-2), 1986.
- Harrison, J.C., Jackson, M.P.A.: Exposed evaporite diapirs and minibasins above a canopy in central Sverdrup Basin, Axel Heiberg Island, Arctic Canada. *Basin Res.* 26, 567–596. <https://doi.org/10.1111/bre.12037>, 2014.
- 525
- Hibbard, S. M., Osinski, G. R., Godin, E.: Vermicular Ridge Features on Dundas Harbour, Devon Island, Nunavut. *Geomorphology*, 395. <https://doi.org/10.1016/j.geomorph.2021.107947>, 2021.
- Holmes, G.W., Hopkins, D.M. and Foster, H.L.: Pingos in central Alaska (p. H1-H40). Washington, DC: US Government
- 530 Printing Office, 1968.
- Hyypä, E., Kukko, A., Kaijaluoto, R., White, J.C., Wulder, M.A., Pyörälä, J., Liang, X., Yu, X., Wang, Y., Kaartinen, H., Virtanen, J.P., Hyypä, J.: Accurate derivation of stem curve and volume using backpack mobile laser scanning. *ISPRS J. Photogramm. Remote Sens.* 161, 246–262. <https://doi.org/10.1016/j.isprsjprs.2020.01.018>, 2020.
- 535
- Johnson, M.D., Clayton, L.: Chapter 10: Supraglacial landsystems in lowland terrain. In: Evans, D.J.A. (Ed.), *Glacial Landsystems*. London, pp. 228–258, 2005.
- Kääb, A., Girod, L., Berthling, I.: Surface kinematics of periglacial sorted circles using structure-from-motion technology. *Cryosphere* 8 (3), 1041–1056. <https://doi.org/10.5194/tc-8-1041-2014>, 2014.
- 540
- Kessler, M.A., Murray, A.B., Werner, B.T., Hallet, B.: A model for sorted circles as self organized patterns. *J. Geophys. Res. Solid Earth* 106 (B7), 13287–13306. <https://doi.org/10.1029/2001JB000279>, 2001.
- 545
- King, C.A. and Buckley, J.T.: Geomorphological investigations in west-central Baffin Island, NWT, Canada. *Arctic and Alpine Research*, 1(2), pp.105-119. <https://doi.org/10.1080/00040851.1969.12003528>, 1969.



- Knudsen, C.G., Larsen, E., Sejrup, H.P., Stalsberg, K.: Hummocky moraine landscape on Jæren, SW Norway-implications for glacier dynamics during the last deglaciation. *Geomorphology* 77, 153–168. <https://doi.org/10.1016/j.geomorph.2005.12.011>, 550 2006.
- Kukko, A., Kaartinen, H., Hyypä, J., Chen, Y.: Multiplatform mobile laser scanning: Usability and performance. *Sensors (Switzerland)*. <https://doi.org/10.3390/s120911712>, 2012.
- 555 Kukko, A., Kaijaluoto, R., Kaartinen, H., Lehtola, V. V., Jaakkola, A., Hyypä, J.: Graph SLAM correction for single scanner MLS forest data under boreal forest canopy. *ISPRS J. Photogramm. Remote Sens.* 132, 199–209. <https://doi.org/10.1016/j.isprsjprs.2017.09.006>, 2017.
- Kukko, A., Kaartinen, H., Osinski, G. and Hyypä, J.: Modeling Permafrost Terrain Using Kinematic, Dual-Wavelength Laser 560 Scanning. *ISPRS Annals of the Photogrammetry, Remote Sensing and Spatial Information Sciences*, 2, 749–756. <https://doi.org/10.5194/isprs-annals-V-2-2020-749-2020>, 2020.
- Lagerbäck, R.: The Veiki moraines in northern Sweden-widespread evidence of an Early Weichselian deglaciation. *Boreas*, 17, 4, 469–486. <https://doi.org/10.1111/j.1502-3885.1988.tb00562.x>, 1988.
- 565 Liestøl, O.: Pingos, springs, and permafrost in Spitsbergen. *Norsk Polarinstittut Årbok*. p. 7-29, 1977.
- Liang, X., Wang, Y., Jaakkola, A., Kukko, A., Kaartinen, H., Hyypä, J., Honkavaara, E., Liu, J.: Forest data collection using terrestrial image-based point clouds from a handheld camera compared to terrestrial and personal laser scanning. *IEEE Trans. Geosci. Remote Sens.* 53, 5117–5132, 2015.
- 570 Lindsay, J.B.: The Whitebox Geospatial Analysis Tools project and open-access GIS. *Proceedings of the GIS Research UK 22nd Annual Conference, The University of Glasgow*, 16-18 April, doi: 10.13140/RG.2.1.1010.8962, 2014.
- 575 Lindsay, J.B.: Whitebox GAT: A case study in geomorphometric analysis. *Computers and Geosciences*, 95: 75–84. doi: 10.1016/j.cageo.2016.07.003, 2016.
- Lundqvist, J.: Rogen (ribbed) moraine—identification and possible origin. *Sedimentary Geology*, 62, 2–4, 281–292. [https://doi.org/10.1016/0037-0738\(89\)90119-X](https://doi.org/10.1016/0037-0738(89)90119-X), 1989.
- 580 Mackay, J.R.: The Mackenzie Delta area, N.W. T.; *Geographical Branch, Memoir* 8, 1963.

Mackay, J.R.: The Mackenzie Delta area, Northwest Territories. Geological Survey of Canada Report 23, Energy, Mines and Resources Canada <https://doi.org/10.4095/119932>, 1974.

585

Mackay, J.R.: Pingo Growth and collapse, Tuktoyaktuk Peninsula Area, Western Arctic Coast, Canada: a long-term field study. *Géog. Phys. Quatern.* 52 (3), 271–323. <https://doi.org/10.7202/004847ar>, 1998.

Mackay, J.R. and Dallimore, S.R.: Massive ice of the Tuktoyaktuk area, western Arctic coast, Canada. *Canadian Journal of Earth Sciences*, 29, 6, 1235–1249. <https://doi.org/10.1139/e92-099>, 1992.

590

Mckenzie, G.D.: Observations on a Collapsing Kame Terrace In Glacier Bay National Monument, South-Eastern Alaska. *J. Glaciol.* 8, 413–425. <https://doi.org/10.3189/s0022143000027003>, 1969.

McKenzie, G.D., Goodwin, R.G.: Development of Collapsed Glacial Topography in the Adams Inlet Area, Alaska, U.S.A. *J. Glaciol.* 33, 55–59. <https://doi.org/10.3189/s0022143000005347>, 1987.

Middleton, M., Heikkonen, J., Nevalainen, P., Hyvönen, E. and Sutinen, R.: Machine learning-based mapping of micro-topographic earthquake-induced paleo-Pulju moraines and liquefaction spreads from a digital elevation model acquired through laser scanning. *Geomorphology*, 358, 107099. <https://doi.org/10.1016/j.geomorph.2020.107099>, 2020.

600

Möller, P., Dowling, T.P.F.: Equifinality in glacial geomorphology: instability theory examined via ribbed moraine and drumlins in Sweden. *GFF* 140 (2), 106–135. <https://doi.org/10.1080/11035897.2018.1441903>, 2018.

Müller, F.: Analysis of some stratigraphic observations and radiocarbon dates from two pingos in the Mackenzie Delta area, NWT. *Arctic*, 15(4), p.279-288, 1962.

605

Ó Cofaigh, C., England, J., Zreda, M.: Late Wisconsinan glaciation of southern Eureka Sound: Evidence for extensive Inuitian ice in the Canadian High Arctic during the Last Glacial Maximum. *Quat. Sci. Rev.* 19, 1319–1341. [https://doi.org/10.1016/S0277-3791\(99\)00104-3](https://doi.org/10.1016/S0277-3791(99)00104-3), 2000.

610

Ó Cofaigh, C., Evans, D., and England, J.: Ice marginal terrestrial landsystems: Sub-polar glacier margins of the Canadian and Greenland high arctic. In *Glacial Landsystems*, Chapter 3, 2005.



- 615 Ó Cofaigh, C., Lemman, D.S., Evans, D.J.A. and Bednarski, J.: Glacial landform-sediment assemblages in the Canadian High Arctic and their implications for late Quaternary glaciations. *Annals of Glaciology*, 28, 195–201. <https://doi.org/10.3189/172756499781821760>, 1999.
- Ommanney, C.S.: A study in glacier inventory: the ice masses of Axel Heiberg Island, Canadian Arctic Archipelago, 1969.
- 620 O'Neill, H.B., Wolfe, S.A. and Duchesne, C.: New ground ice maps for Canada using a paleogeographic modelling approach. *The Cryosphere*, 13(3), p.753-773. <https://doi.org/10.5194/tc-13-753-2019>, 2019.
- Paulen, R.C., McClenaghan, M.B.: Late wisconsin ice-flow history in the buffalo head hills kimberlite field, north-central alberta. *Can. J. Earth Sci.* 52 (1), 51–67. <https://doi.org/10.1139/cjes-2014-0109>, 2014.
- 625 Pissart, A., French, H.M.: Pingo investigations, north-central Banks Island, Canadian Arctic. *Can. J. Earth Sci.* 13 (7), 937–946. <https://doi.org/10.1139/e76-096>, 1976.
- 630 Pissart, A., French, H.M.: The origin of pingos in regions of thick permafrost, western Canadian Arctic. *Quaestiones Geographicae* 4, 149–160. <http://hdl.handle.net/2268/248067>, 1977.
- Pollard, W. H.: Distribution and characterization of ground ice on Fosheim Peninsula, Ellesmere Island, Nunavut, in: *Environmental response to climate change in the Canadian High Arctic*, edited by: Garneau, M. and Alt, B. T., Geological Survey of Canada, Ottawa, ON, Canada, Bulletin 529, 207–233, 2000.
- 635 Pollard, W. and Bell, T.: Massive ice formation in the Eureka Sound Lowlands: A landscape model. In *Proceedings, Seventh International Permafrost Conference* (pp. 903-908). Laval, Quebec City, Quebec, Canada: Université Laval, Centre d'études nordiques, Collection Nordicana, 1998.
- 640 Pollard, W., Omelon, C., Andersen, D., McKay, C.: Perennial spring occurrence in the Expedition Fiord area of western Axel Heiberg Island, Canadian High Arctic. *Can. J. Earth Sci.* 36, 105–120. <https://doi.org/10.1139/e98-097>, 1999.
- Porter, C., Morin, P., Howat, I., Noh, M., Bates, B., Peterman, K., Keesey, S., Schlenk, M., Gardiner, J., Tomko, K., Willis, M., Kelleher, C., Cloutier, M., Husby, E., Foga, S., Nakamura, H., Platson, M., Wethington, M. J., Williamson, C., Bauer, G., Enos, J., Arnold, G., Kramer, W., Becker, P., Doshi, A., D'Souza, C., Cummens, P., Laurier, F., Bojesen, M.: ArcticDEM. <https://doi.org/10.7910/DVN/OHHUKH>, (Harvard Dataverse, V1), (accessed 23 May 2022), 2018.



- 650 Rampton, V. N.: Quaternary Geology of the Tuktoyaktuk Coastlands, Northwest Territories, Memoir 423, Geological Survey of Canada, Ottawa, ON, Canada, 1988.
- Ross, N., Brabham, P., Harris, C.: The glacial origins of relict “pingos”, Wales, UK. *Ann. Glaciol.* 60, 138–150. <https://doi.org/10.1017/aog.2019.40>, 2019.
- 655 Russell, A.J., Roberts, M.J., Fay, H., Marren, P.M., Cassidy, N.J., Tweed, F.S., Harris, T.: Icelandic jökulhlaup impacts: Implications for ice-sheet hydrology, sediment transfer and geomorphology. *Geomorphology* 75, 33–64. <https://doi.org/10.1016/j.geomorph.2005.05.018>, 2006.
- Schmertmann, J.H., Taylor, R.S.: Quantitative data from a patterned ground site over permafrost. U.S. Army Cold Regions Research and Engineering Laboratory Research Report. 96, p. 76, 1965.
- 660
- Sutinen, R., Hyvönen, E., Middleton, M., Ruskeeniemi, T.: Airborne LiDAR detection of postglacial faults and Pulju moraine in Palojärvi, Finnish Lapland. *Glob. Planet. Chang.* 115, 24–32. <https://doi.org/10.1016/j.gloplacha.2014.01.007>, 2014.
- 665 Sutinen, R., Hyvönen, E., Middleton, M., Airo, M.L.: Earthquake-induced deformations on ice-stream landforms in Kuusamo, eastern Finnish Lapland. *Glob. Planet. Chang.* 160, 46–60. <https://doi.org/10.1016/j.gloplacha.2017.11.011>, 2018.
- Sutinen, R., Hyvönen, E., Liwata-Kenttälä, P., Middleton, M., Ojala, A., Ruskeeniemi, T., Sutinen, A., Mattila, J.: Electrical-sedimentary anisotropy of landforms adjacent to postglacial faults in Lapland. *Geomorphology* 326, 213–224. <https://doi.org/10.1016/j.geomorph.2018.01.008>, 2019.
- 670
- Taylor, A.E., Judge, A.S.: Canadian Geothermal Data Collection: Northern Wells. Ottawam, 1976.
- Thomson, L.I., Osinski, G.R., Ommanney, C.S.L.: Glacier change on Axel Heiberg Island, Nunavut, Canada. *J. Glaciol.* 57, 1079–1086. <https://doi.org/10.3189/002214311798843287>, 2011.
- 675
- Thorsteinsson, R.: Geology, Eureka Sound North, District of Franklin. Geological Survey of Canada, "A" Series Map 1302A, 1 sheet, <https://doi.org/10.4095/109125>, 1971a.
- 680 Thorsteinsson, R.: Geology of Strand Fiord, District of Franklin. Geological Survey of Canada, Map 1301A, scale 1:250 000, 1971b.

Washburn, A.L.: Classification of patterned ground and review of suggested origins. *Bull. Geol. Soc. Am.* 67 (7), 823–865.
[https://doi.org/10.1130/0016-7606\(1956\)67\[823:COPGAR\]2.0.CO;2](https://doi.org/10.1130/0016-7606(1956)67[823:COPGAR]2.0.CO;2), 1956.

685

Washburn, A.: *Periglacial Processes and Environments*. Edward Arnold, London, 1973.

Wolfe, S.A., Stevens, C.W., Gaanderse, A.J. and Oldenborger, G.A.: Lithalsa distribution, morphology and landscape associations in the Great Slave Lowland, Northwest Territories, Canada. *Geomorphology*, 204, p. 302-313.

690 <https://doi.org/10.1016/j.geomorph.2013.08.014>, 2014.